

An Introduction to the EVN

T. W. B. Muxlow¹

Jodrell Bank Centre for Astrophysics

Alan Turing Building, University of Manchester, Oxford Road, Manchester M13 9PL, United Kingdom

E-mail: tom.muxlow@manchester.ac.uk

In recent years the European VLBI Network has expanded significantly with many new large telescopes in across continents resulting in much enhanced sensitivity and new Global resolving power – the EVN now has > 10% of the planned SKA phase 1 collecting area on baselines of thousands of kilometres. This enhancement has led to a surge in user demand and oversubscription rates – only the very best science can now get time on the EVN. This together with the rapid response of e-VLBI has produced a significant number of recent high profile scientific results.

In this presentation, I will give an introduction and overview to the enhanced EVN array and review some recent science highlights – with reference to a number of exciting current programmes which are being reported at this latest EVN Symposium.

References from which I have drawn most of the material are shown red in the text.

*11th European VLBI Network Symposium & Users Meeting
October 9-12, 2012
Bordeaux, France*

¹ Speaker

1. Outline

EVN capabilities – What does the expanded EVN offer the prospective astronomical user?

Proposal trends and research areas over the last 6 years – What research areas does the current astronomical community address in their past and present EVN proposals?

Some recent published results and current notable work:

Astrometry

Stellar evolution

AGN jets

Nearby galaxies

Radio quasars at early cosmological epoch

2. EVN Capabilities

With the recent expansion of the EVN, the total collecting area now available to prospective users, involving > 20 large antennas across the world (Fig. 1), is now in excess of 10% of the planned SKA phase 2. The EVN is now indeed a genuine SKA pathfinder instrument.

With such a large collecting area and wide bandwidth recording (up to 1 Gbps), and with baselines $> 10^4$ km, the EVN now routinely delivers microJansky sensitivity together with sub-milliarcsecond angular resolution.

With many telescopes worldwide, the expanded EVN delivers high image fidelity derived from the excellent u - v (spatial frequency) coverage.

Accurate timing at each site from hydrogen masers and state-of-the-art stable receiver systems deliver good phase stability which in turn gives the EVN superb astrometric capability with positional accuracy approaching 100 microarcseconds (μ as).

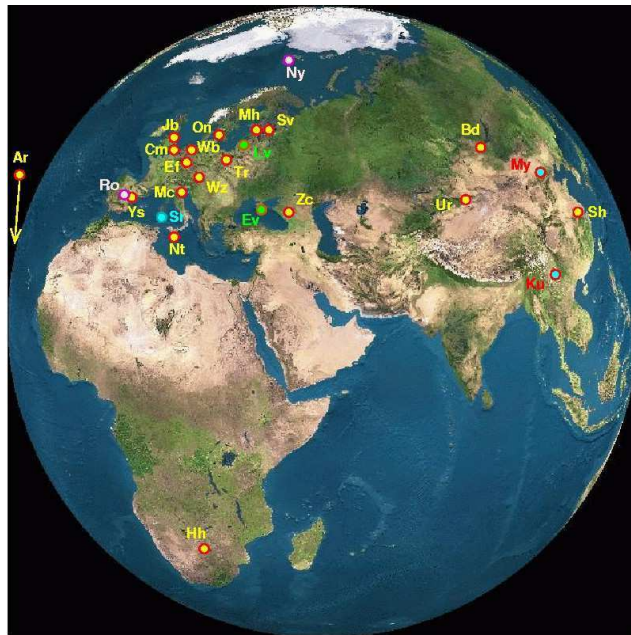


Figure 1. The EVN array, incorporating Global baselines $> 10^4$ km.

3. Proposal trends and research areas over the last 6 years

With the expansion of the array, the submitted EVN astronomical proposal totals (Fig. 2) have nearly doubled in 6 years – dominated by increases in proposed conventional disk-based EVN time. e-VLBI has stabilized at about 20% of proposal numbers, with Global proposal numbers about 9/year throughout. The typical oversubscription rate now stands at 2.2.

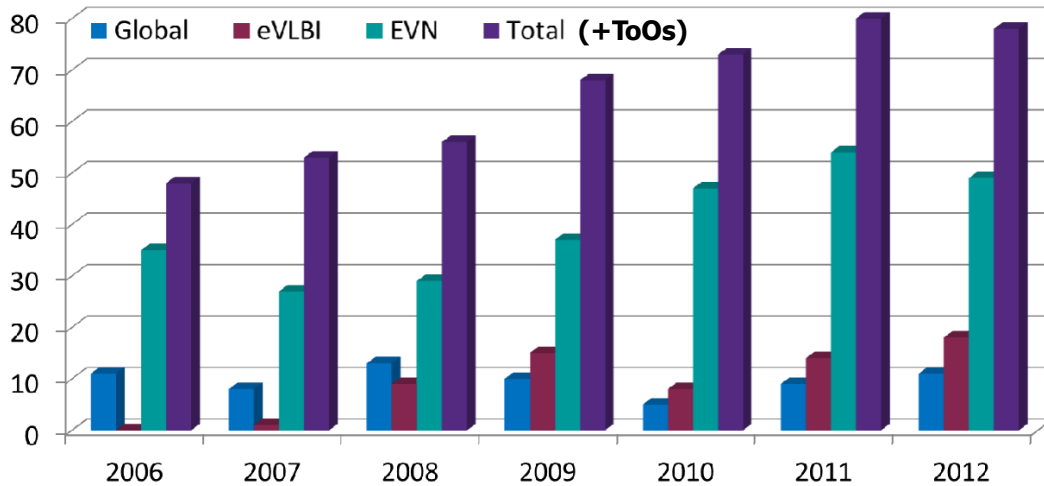


Figure 2. Submitted proposals from 2006-2012 encoded by proposal type.

The breakdown of the submitted proposal science areas over the past two years (Fig. 3) is still dominated by classical areas of AGN/jets, stellar evolution, and starburst/ULIRGs (ultra-luminous infrared galaxies) – with a healthy maser community and more specialized astrometry and spacecraft tracking programmes.

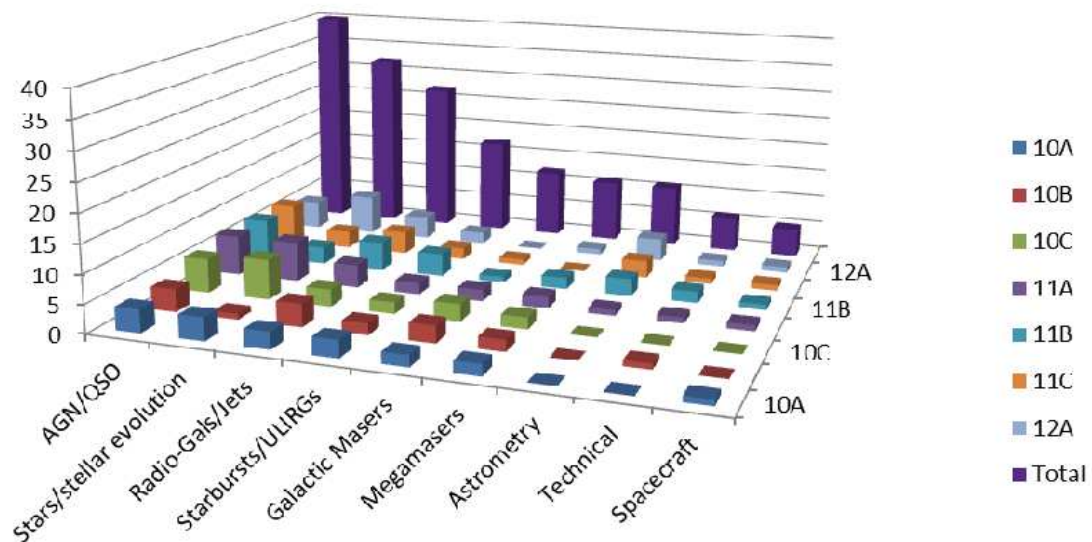


Figure 3. Breakdown of proposal science areas over the past two years.

4. Astrometry

The EVN now has well-established astrometric credentials with very high sensitivity which are now routinely applied to both near space and cosmic distance scales.

Within the solar system, the EVN is being used for high-sensitivity current and future (e.g. Venus Express) spacecraft tracking missions to enhance the scientific returns of the spacecraft primary programmes – now firmly established following the dramatic successes of the VLBI astrometric tracking of the Huygens probe during its descent onto the surface of Titan on 14 January 2005 (Fig. 4). VLBI recovered the probe’s position with a precision of 0.5 x 2.0 km (semi-axes of the error scatter ellipse) in projection onto Titan’s surface allowing the spacecraft velocity to be measured to 3.5 +/- 0.5 m/s – showing 400 km/s atmospheric winds 150 km above the surface [12].

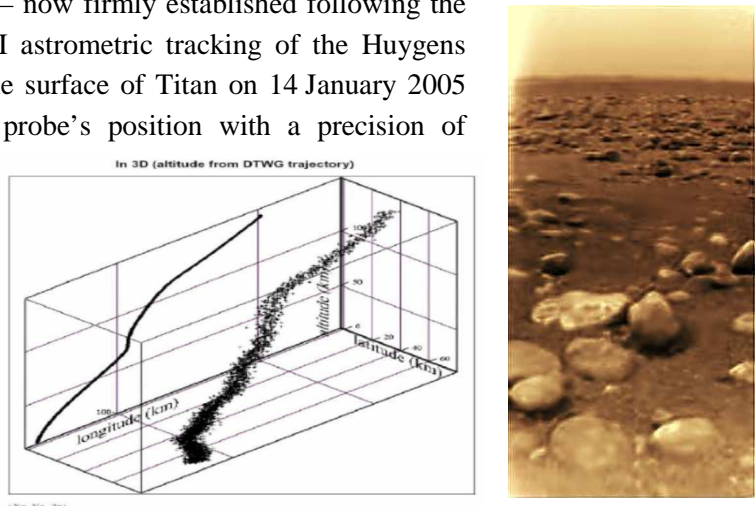


Figure 4. *Left:* descent trajectory of the Huygens probe. *Right:* image of Titan’s surface from Huygens.

Pogrebenko et al. 2009 [12]

Plans to tie the radio-based ICRF (International Celestial Reference Frame) and the future optically-based Gaia celestial reference frame with the precision found within each frame (a few tens of μ as) are based on VLBI astrometry. Gaia is an ESA project due for launch in August 2013 (Fig. 5). This is a successor to the Hipparcos mission which aims to compile a catalogue of 1 billion stars, about 1% of the stars in the Milky Way.

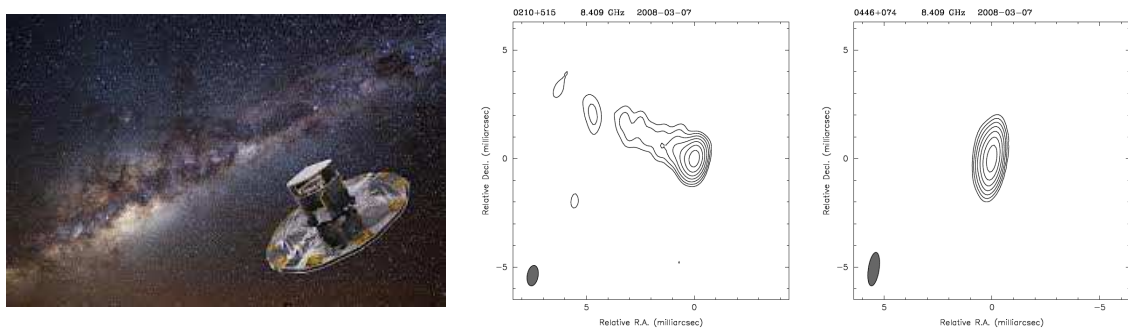


Figure 5. *Left:* artist’s impression of the Gaia spacecraft. *Right:* examples of unsuitable (left) and suitable (right) radio structures found by recent Global VLBI observations at 8.4 GHz.

Initial observations have started to select quasar candidates which are compact (no extended jets) in the radio, and bright enough (< 18th mag) for Gaia to derive an accurate optical position (Fig. 5) [5, 6]. Proposed Global VLBI astrometry will tie the Gaia frame to the ICRF.

Bourda et al. 2011 [5]

5. Stellar evolution

22 GHz water masers are often associated with 6.7 GHz methanol masers but owing to the different excitation conditions they probe independent spatial and kinematic regions powering young massive stars, whose star formation process is poorly as yet understood. Bartkiewicz, Szymczak, and van Langevelde [2] have compared the emission of these two maser species on milliarcsecond scales with the EVN around two high-mass young stellar objects (G31.581+00.77 and G33.64-00.228) to determine in which structures the masers arise and to test a disk-outflow scenario where the methanol emission arises in a circumstellar disk while the water emission comes from an outflow.

In both targets the main axis of methanol maser distribution is orthogonal to the water maser distribution and the methanol spots appear to be associated with a circumstellar disk while the water emission comes from an outflow/jet (Fig. 6). The H₂O masers appear to trace shocks on a working surface between an outflow/jet and a dense envelope, and some spots are possibly related to the disk-wind interface.

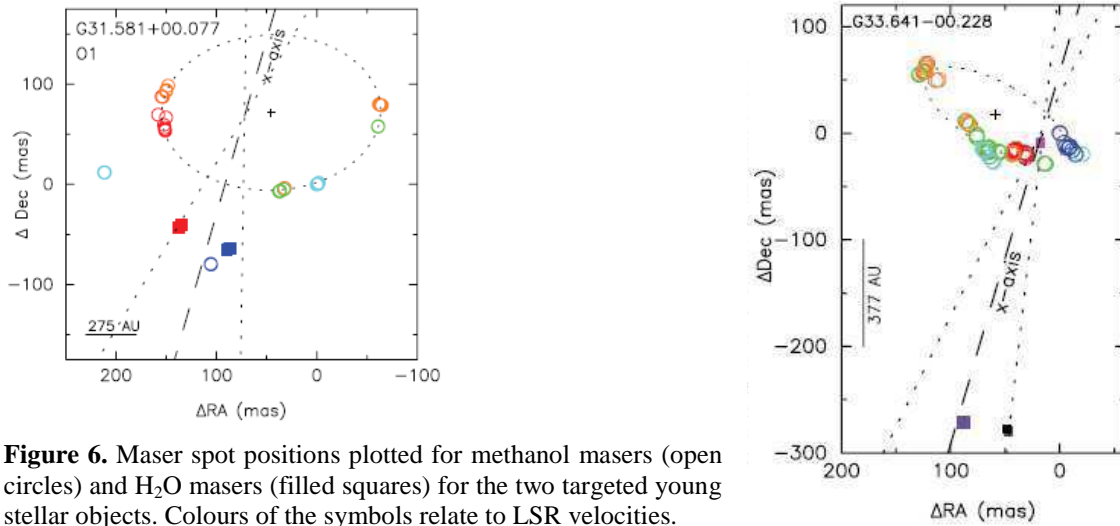
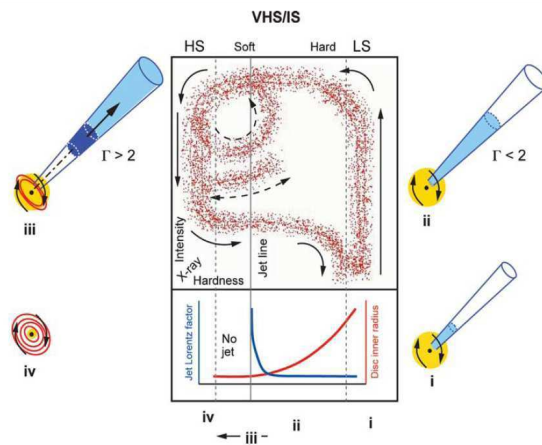


Figure 6. Maser spot positions plotted for methanol masers (open circles) and H₂O masers (filled squares) for the two targeted young stellar objects. Colours of the symbols relate to LSR velocities.

[Bartkiewicz et al. 2012 \[2\]](#)

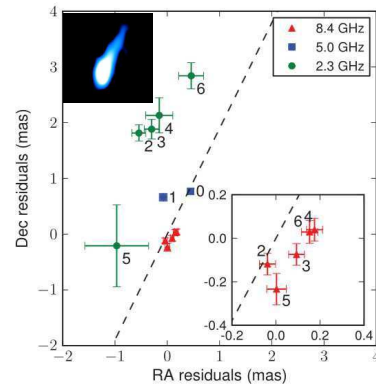
The EVN with its high sensitivity and angular resolution is the instrument of choice for the study of Galactic X-ray binary systems – particularly the details of the X-ray binary state diagram (Fig. 7) with regard to the disk-jet connection in accreting black hole systems.

Figure 7. The X-ray binary state diagram [8]. In outburst, sources cycle through states i → iv, starting at bottom right and moving anti-clockwise. Bright fast radio jets appear as the ‘jet line’ is crossed during periods when the Lorentz factor is high and as the radius of the inner accretion disk collapses. Multiple outbursts cross this line several times.



With respect to the state diagram, sources in outburst tend to cycle through states $i \rightarrow ii \rightarrow iii \rightarrow iv$ with associated changes in X-ray hardness and luminosity. The radio appearance is characterised by variations in accretion disk radiation absorption and inner accretion disk radius.

Figure 8. Residual astrometric VLBI positions of Cygnus X-1 in July 2010 when in the low hard state. Longer wavelength positions are systematically offset due to a frequency dependence of the fitted position for the phase reference calibrator. Inset (top left): Global VLBI image of Cygnus X-1 during outburst showing jet position angle.



It had been thought that no jet was present during the faint soft state (iv) since none had ever been detected. However, a recent detailed e-EVN and VLBA astrometric study of Cygnus X-1 [13] over a period of 14 days in June 2010 (Fig. 8) showed that the soft state faint compact radio component has a scatter in position along the position angle found in the low hard state (i) indicating that the jet must still be present. X-ray binary systems are now routinely studied with the EVN – and the data and images are used to provide strong constraints on the detailed flaring models.

Rushton et al. 2012 [13]

6. AGN jets

In May 2005 a high-energy X-ray outburst was detected in the region of a knot in the M87 jet. The feature, HST-1 (Fig. 9), was seen to vary on a timescale of ~ 200 days. The role of HST-1 has been studied with respect to the structure of the kpc-scale jet by Asada & Nakamura [1], while its kinematics have been studied in detail by Giroletti et al. [10].

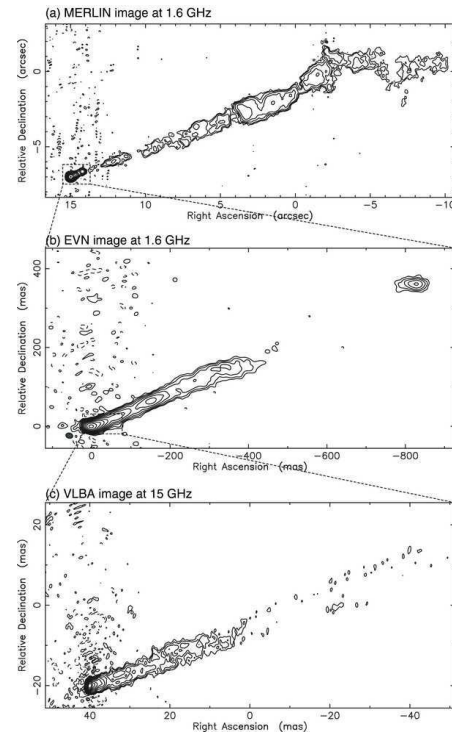
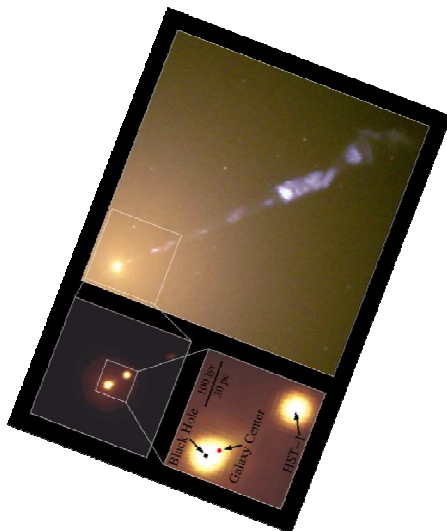


Figure 9. *Left:* HST images of the HST-1 region (STScI/AURA, Biretta, Sparks, Macchetto, & Perlman). *Right:* images of the M87 jet at 1.6 GHz from MERLIN and the EVN, and at 15 GHz with the VLBA [1].

Asada & Nakamura [1] have used MERLIN 1.6 GHz data from March 2007, EVN 1.6 GHz data from March 2009, and archival pre-HST-1 VLBA 15 GHz data from January 2000 (Fig. 9) together with a published composite 43 GHz VLBA image (Fig. 10) to explore the changes in jet opening angle with position along the kpc-scale jet in M87 (Fig. 10).

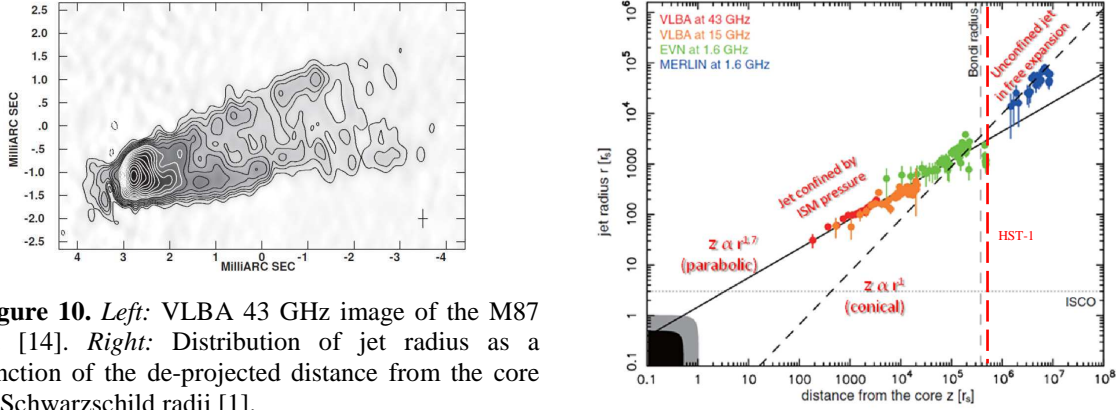


Figure 10. *Left:* VLBA 43 GHz image of the M87 jet [14]. *Right:* Distribution of jet radius as a function of the de-projected distance from the core in Schwarzschild radii [1].

The HST-1 feature lies near the Bondi radius – the point where the accreting gas becomes supersonic. Upstream of HST-1 the jet streamlines are parabolic, indicating that the jet is confined by the gas pressure of the ISM. Downstream the streamlines are conical indicating the jet is unconfined and in free expansion laterally. Asada & Nakamura [1] argue that if HST-1 is associated with the Bondi radius, then the feature could well be a re-collimation shock where there is a change in the ISM pressure profile. The HST-1 knot would thus be the result of jet over-collimation and is likely to be a stationary feature through which the jet material passes.

Asada & Nakamura 2012 [1]

The kinematics of HST-1 in the jet of M87 have been studied by Giroletti et al. [10] through detailed monitoring with the EVN (6 cm, 13 epochs) and the VLBA (18 cm) since 2007 (Fig. 11). They show that the substructure in HST-1 has evolved with changes in overall position angle with superluminal jet components ($\sim 4c$) passing through what appears to be a stationary feature, possibly a re-collimation shock.

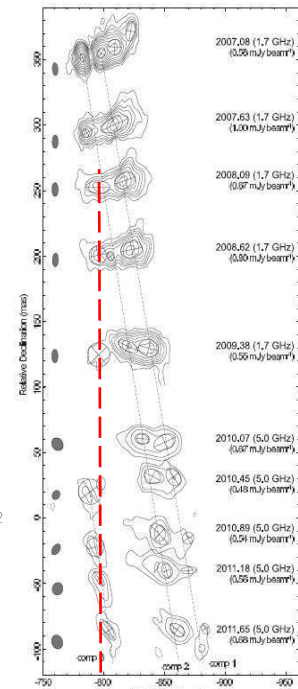
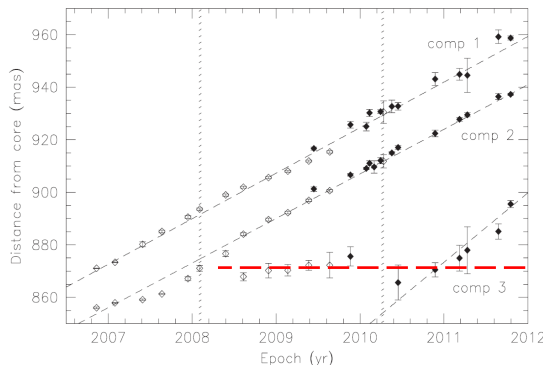


Figure 11. *Left:* motion of jet components through HST-1 position. *Right:* HST-1 region showing evolving structure and position angle with time. HST-1 position is shown in red.

Giroletti et al. 2012 [10]

7. Nearby galaxies

7.1 SNR monitoring in M82

Following the appearance of a new supernova in M82 (SN2008iz), thought to have exploded on 20 February 2008, extensive high-resolution monitoring has taken place in the radio bands with the VLBA, HSA, and e-EVN [7]. The images reveal a shell-like structure with circular symmetry, expanding in a self-similar way (Fig. 12). There is also strong evidence of a compact component with a steep spectrum at the centre of the shell, detected at 5 GHz, but at higher frequencies. A similar compact component was detected also in the centre of the SN1986J radio shell [3], which the authors identified as either pulsar emission or related to accretion onto a black hole – this may be another example.

The expansion curve obtained from the VLBI observations (Fig. 12) shows marginal deceleration with an expansion index of 0.89. The initial expansion velocity is $\sim 21\,000$ km/s. The structure can be modeled simultaneously with the available radio light curves and exhibits properties typical for a Type II SNe. Detailed VLBI monitoring is continuing.

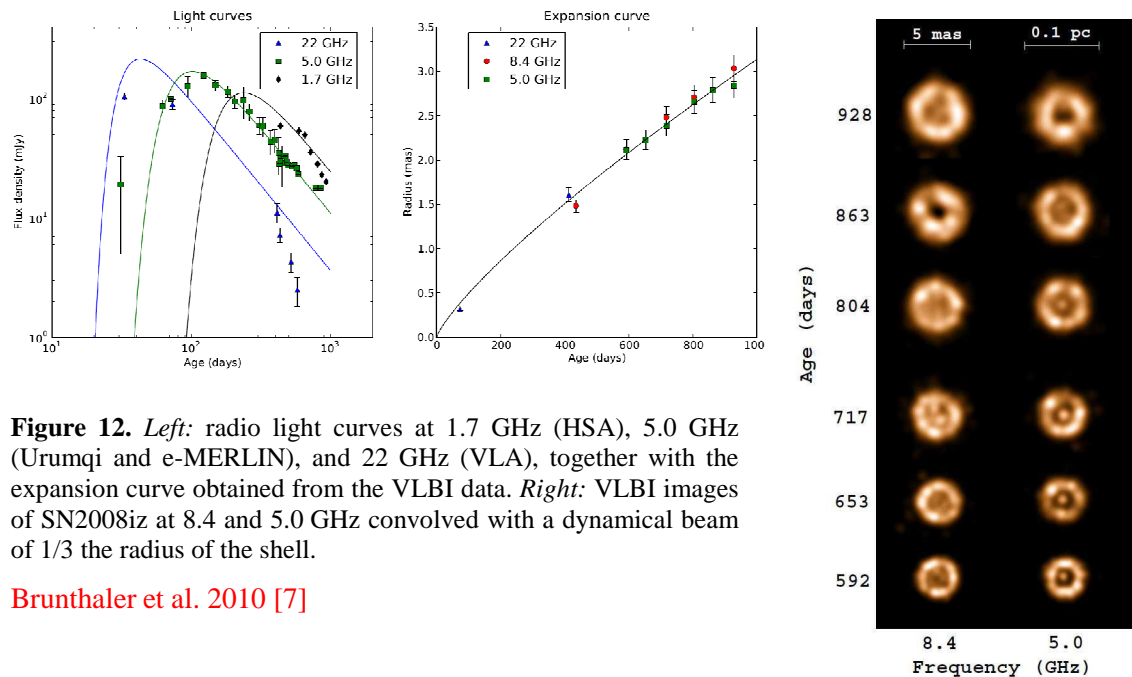


Figure 12. *Left:* radio light curves at 1.7 GHz (HSA), 5.0 GHz (Urumqi and e-MERLIN), and 22 GHz (VLA), together with the expansion curve obtained from the VLBI data. *Right:* VLBI images of SN2008iz at 8.4 and 5.0 GHz convolved with a dynamical beam of $1/3$ the radius of the shell.

Brunthaler et al. 2010 [7]

7.2 The nuclear starburst in Arp 299-A

Arp 299 is a luminous infrared galaxy at a distance of 45 Mpc. The recent intense starburst activity has been triggered by a tidal interaction between IC694 and NGC3690 (Fig. 13). Bondi et al. [4] have used the EVN at 6 cm to monitor Arp 299-A (IC694) every 6 months since April 2008 and have stacked their multi-epoch maps to produce the deepest ever 6 cm image of Arp 299-A (Fig. 14).

An analysis of the temporal and spectral evolution of the compact sources in the deep EVN image indicates that they are mostly a mixture of young core-collapsed radio SNe and SNRs. The rate at which new SNe appear allows an estimate of the core-collapse SN rate to be made yielding a lower limit of > 0.80 SN/yr within the innermost 150 pc.

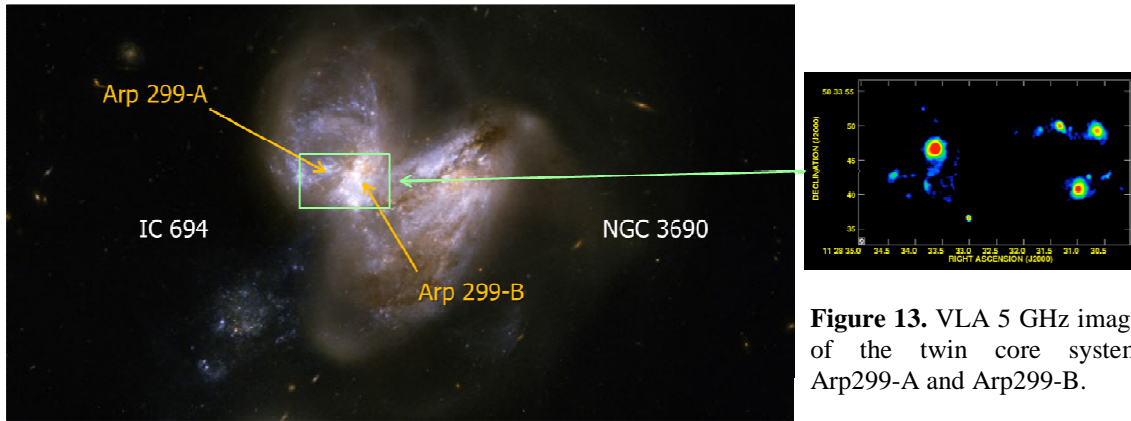


Figure 13. VLA 5 GHz image of the twin core system Arp299-A and Arp299-B.

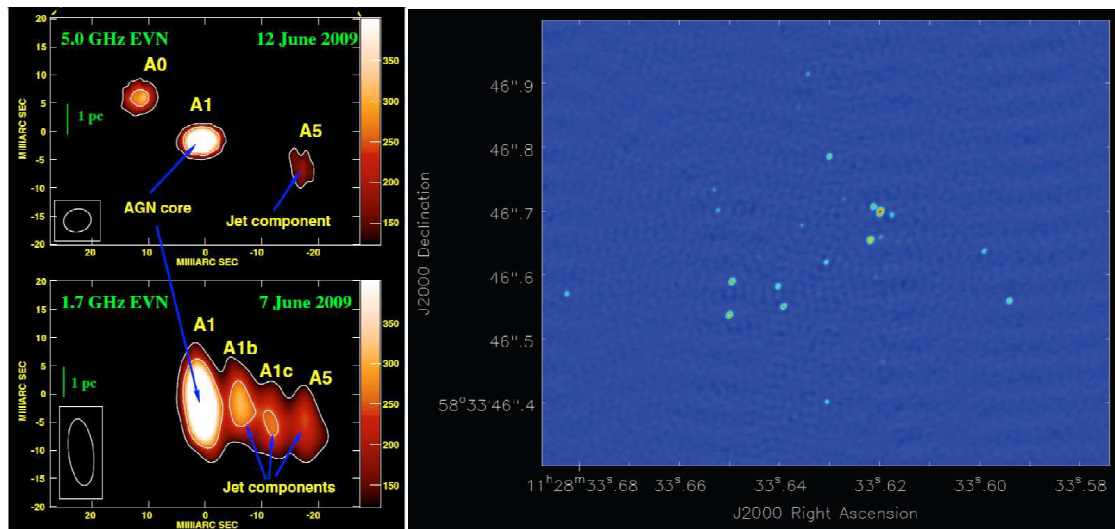


Figure 14. Left: upper panel: EVN 5 GHz image of the central AGN in Arp299-A; lower panel: EVN 1.7 GHz image showing the central core and the associated jet in Arp299-A. Right: stacked multi-epoch 5 GHz EVN image of Arp299-A.

Components A1 and A5 in Fig. 14 have previously been identified as an AGN core-jet structure [11], indicating that Arp299-A is a composite starburst and low-luminosity AGN system.

[Bondi et al. 2012 \[4\]](#)

8. Radio quasars at early cosmological epoch

The programme to study radio quasars at early cosmological epoch is a development of an existing EVN study – now extended to quasars at redshifts > 6 [9]. Among the known $z \sim 6$ quasars, $< 10\%$ are radio-emitting and have steep spectra. As found previously, these quasars show structure on 10-100 pc linear scales (see e.g. J1429+5447 in Fig. 15). Many of the highest redshift quasars ($z > 6$) are doubles, and are similar to low-redshift compact symmetric objects. The highest-redshift radio quasars are still very rare implying that there are many more, just waiting for discovery. Quasars at such high redshifts are sampling the epoch close to the end of the era of re-ionization, and as such are radio beacons for sensitive HI absorption studies.

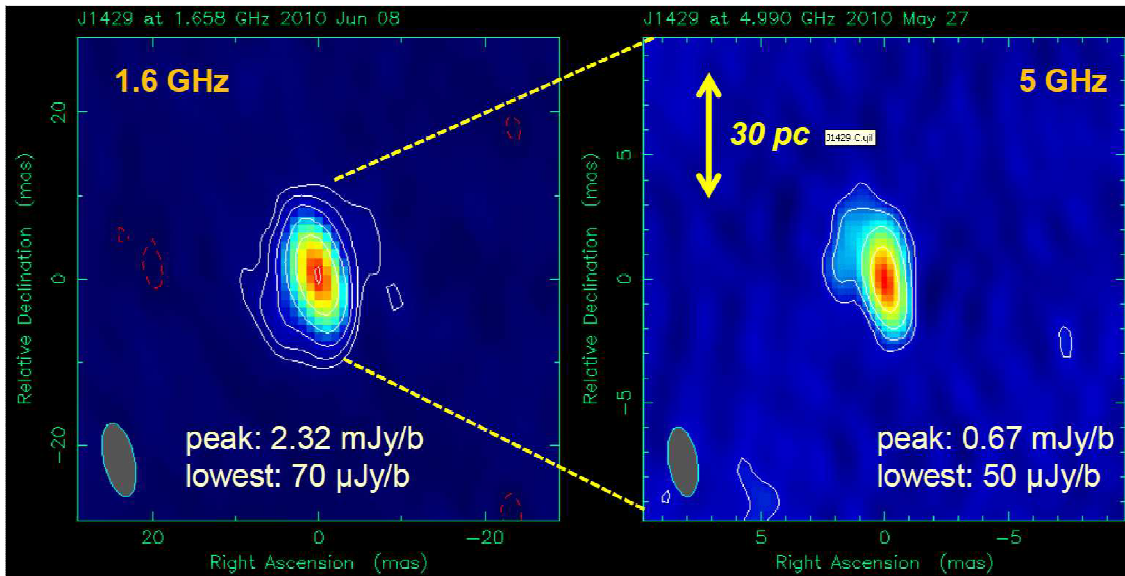


Figure 15. EVN images of the high-redshift quasar J1429+5447 ($z = 6.21$) at 1.6 and 5 GHz.

Frey et al. 2011 [9]

References

- [1] Asada, K., & Nakamura, M. 2012, ApJ, 745, L28
- [2] Bartkiewicz, A., Szymczak, M., & van Langevelde, H. J. 2012, A&A, 541, A72
- [3] Bietenholz, M., Bartel, N., & Rupen, M. 2004, Science, 304, 1947
- [4] Bondi, M., Pérez-Torres, M., Herrero-Illana, R., & Alberdi, A. 2012, A&A 539, A134
- [5] Bourda, G., Collioud, A., Charlot, P., Porcas, R., & Garrington, S. 2011, A&A, 526, A102
- [6] Bourda, G., Collioud, A., Charlot, P., Porcas, R., & Garrington, S. 2012, MmSAI, 83, 966
- [7] Brunthaler, A., Marti-Vidal, I., Menten, K., et al. 2010, PoS (10th EVN Symposium) 055
- [8] Fender, R. 2004, NewAR, 48, 1399
- [9] Frey, S., Paragi, Z., Gurvits, L., Gabányi, K., & Cseh, D. 2011, A&A, 531, L5
- [10] Giroletti, M., Hada, K., Giovannini, G., et al. 2012, A&A, 538, L10
- [11] Pérez-Torres, M., Alberdi, A., Romero-Cañizales, C., & Bondi, M. 2010, A&A, 519, L5
- [12] Pogrebenko, S., Gurvits, L., Avruch, I., & Cimo, G. 2009, ESPC Abst., 4, 199
- [13] Rushton, A., Miller-Jones, J., Campana, R., et al. 2012, MNRAS, 419, 3194
- [14] Walker, R., Ly, C., Junor, W., & Hardee, P. 2008, ASP Conf. Ser., 386, 87